

Glacial retreat and rising temperatures are limiting the expansion of temperate kelp species in the future Arctic

Sarina Niedzwiedz ,* Kai Bischof 

Marine Botany, Faculty of Biology and Chemistry & MARUM, University of Bremen, Leobener Straße NW2, Bremen, Bremen, 28359, Germany

Abstract

Kelps act as ecosystem engineers on many polar rocky shore coastlines. The underwater light climate and temperature are the main drivers for their vertical and latitudinal distribution. With temperatures rising globally, an Arctic expansion of temperate kelp species and an accelerating glacial melt is predicted. It was our aim to investigate the effects of retreating glaciers and rising temperatures on the potential habitat of kelps in Arctic fjords. We analyzed the underwater light climate of areas being influenced by different stages of glacial retreat (sea-terminating glacier, land-terminating glacier, coastal water) in Arctic Kongsfjorden. We observed reduced light intensities and a changed spectral composition in glacial meltwater plumes, potentially resulting in an upward shift of the lower depth limit of kelp, counteracting the predicted biomass increase in the Arctic. Furthermore, we studied temperature-related changes in light-use characteristics in two kelp species (*Alaria esculenta*, *Saccharina latissima*) at 3°C, 7°C, and 11°C. Rising temperatures lead to a significant increase of the compensation irradiance of *A. esculenta*. The dark respiration of *S. latissima* increased significantly, correlating with a decreasing carbon content. We detected no differences in photosynthetic rates, although the chlorophyll *a* concentration of *A. esculenta* was ~ 78% higher compared to *S. latissima*. Ultimately, temperature-induced changes in kelps light-use characteristics might lead to a changed species composition, as we found *A. esculenta* better adapted to polar conditions. We conclude that the deterioration of the underwater light climate and the temperature increase may drive substantial changes of the future Arctic kelp forest structure.

Kelps (Laminariales, Phaeophyceae) dominate many rocky shore coastlines in temperate and polar regions, forming sub-marine forests that are among the most productive ecosystems on our planet (Teagle et al. 2017; Wernberg et al. 2019). Kelps function as ecosystem engineers and foundation species, thereby providing a wide range of ecosystem services that are of vast socioeconomic importance (Eckman et al. 1989; Filbee-Dexter et al. 2019; Wernberg et al. 2019). However, kelp forest distribution and productivity strongly depend on external

biotic and abiotic factors (e.g., Feehan et al. 2012; Smale and Wernberg 2013; Smale 2020). Especially in the context of global climate change, it is important to understand the drivers of kelp forest distribution to conserve these ecosystems and their essential ecological and socioeconomic role.

The underwater light climate, being defined as the intensity of photosynthetically active radiation (PAR) and the spectral composition of the downwelling irradiance, is a key driver of kelps vertical distribution in the water column (Wondraczek et al. 2013; Fragkopoulou et al. 2022). Kelps are dependent on the underwater light climate as they can only accumulate biomass, if their net carbon uptake (photosynthesis) exceeds their carbon loss (respiration), that is, if their net photosynthetic rate is positive (Kirk 2011). The light intensity at which the photosynthetic and respiration rate are balanced is called compensation irradiance. Its ecological application is the compensation depth, above which net carbon uptake is positive and below it is negative (Falkowski and Raven 2007). The underwater light climate is the result of complex interactions, such as the Sun's activity, the Earth orbit geometry and the light transmission through the atmosphere (Kirk 2011), as well as spectral properties of the water and its suspended particles, scattering and absorbing light (Stomp et al. 2007).

*Correspondence: sarina@uni-bremen.de

This is an open access article under the terms of the [Creative Commons Attribution-NonCommercial](https://creativecommons.org/licenses/by-nc/4.0/) License, which permits use, distribution and reproduction in any medium, provided the original work is properly cited and is not used for commercial purposes.

Additional Supporting Information may be found in the online version of this article.

Author Contribution Statement: S.N. and K.B. planned the study and experiments. S.N. and K.B. measured the underwater light climate in Kongsfjorden in July 2021. S.N. conducted the temperature experiment, evaluated the data and wrote the manuscript, which was revised, reviewed and accepted by K.B. S.N. and K.B. interpreted and discussed the data. K.B. supervised the project.

The influence of suspended particular matter is particularly pronounced in the Arctic (Aksnes et al. 2009; Konik et al. 2021), as permafrost thaw (Bintanja 2018), melting glaciers (Milner et al. 2017) and high precipitation rates (Bintanja and Andry 2017) release sediments to fjord systems. The sediment concentration of the fjord meltwater layer is heterogeneous with spatial and temporal (seasonal) variations (Huovinen et al. 2020), which are strongly affected by the glacier type. At sea-terminating glaciers, the meltwater enters the ocean below the surface and rises buoyantly toward the surface once it reaches open water, establishing an upwelling nutrient flux. As the meltwater of land-terminating glaciers discharges into proglacial rivers, entering the fjord on the surface (Schild et al. 2017), this nutrient flux subsides once the glacier becomes land-terminating. Furthermore, the sediment plume dynamics affect the sedimentation patterns. This has consequences to kelp population dynamics and interspecific competition (Traiger and Konar 2017), as the substrate quality and the properties of the downwelling irradiance, reaching the benthos are changed (Huovinen et al. 2020). Whether the effect of glacial retreat and run-off on marine primary production is positive or negative depends on a multitude of interacting factors, for example, fjord-glacier geometry, resource availability, and glacier type (Hopwood et al. 2020). In the near-future, the loss of global glacier mass is predicted to accelerate (Hugonnet et al. 2021), resulting in increasing terrestrial run-off (Bintanja and Andry 2017), sediment release and, consequently, a deterioration of the underwater light climate (Payne and Roesler 2019).

Temperature is a key driver of the latitudinal distribution of kelps (Fragkopoulou et al. 2022). Since the past century, the annual mean global sea surface temperature (SST) is rising drastically (Xu et al. 2021) and sedentary species, such as kelps, have to adapt to thrive under future conditions (Vranken et al. 2021). For many kelp species, rising SSTs have already led to a high mortality at their warm-distribution edge (Krumhansl et al. 2016; Filbee-Dexter et al. 2020) and a poleward range shift of kelps has been recorded (Smale and Wernberg 2013; Bartsch et al. 2016). For many kelp species, SSTs in the Arctic are currently below their optimum growth temperature (Krause-Jensen et al. 2020). Therefore, the species trait characteristics to survive and produce viable offspring in the Arctic environmental setting is not optimal (reduced performance; Pörtner et al. 2005). Hence, kelp biomass accumulation in the Arctic is lower compared to mid-latitudinal regions (Borum et al. 2002; Pessarrodona et al. 2018). However, with the Arctic warming at a rate far beyond the global average (Previdi et al. 2020, 2021; England et al. 2021), near-future SSTs might allow for increasing enzymatic activity and performance (Pörtner et al. 2005). Consequently, models predict a biomass increase of kelps in the Arctic (Krause-Jensen and Duarte 2014; Krause-Jensen et al. 2020; Assis et al. 2022). However, higher temperatures were shown to alter species light-use characteristics (Davison et al. 1991; Atkin and Tjoelker 2003), this might result in rising compensation

irradiance. Depending on the species temperature tolerance, temperature changes affect species light-use characteristics differently, which might result in a changed species community composition (Traiger and Konar 2017).

It was the aim of this study to gain a mechanistic understanding of the interactive effects of deteriorating underwater light climate and rising SSTs in Arctic fjords on the potential habitat of the two cold-temperate kelp species *Alaria esculenta* and *Saccharina latissima*. Both species are forming extensive kelp forests in Kongsfjorden, Svalbard (Bartsch et al. 2016), which is at their cold-distribution edge with summer SSTs below their optimum growth temperature (Munda and Lüning 1977; Bolton and Lüning 1982). We assessed the influence of glacial retreat on the underwater light climate and the effect of temperature on the light-use characteristics of kelps. Our study was guided by two hypotheses:

Hypothesis 1: Given the complex sediment plume dynamics of sea- and land-terminating glacier, we expect a strong spatial gradient of prevailing PAR intensities, decreasing closer to the glaciers, which results in a shallower compensation depth of kelps.

To verify this, we chose Kongsfjorden, Svalbard as model fjord system, analyzing the underwater light climate in three areas, representing different stages of glacial retreat: (1) sea-terminating glacier, (2) land-terminating glacier, (3) coastal water (at the mouth of the fjord). Based on these results, we created a model showing the prevailing PAR intensities in Kongsfjorden. Furthermore, we expect the spectral composition to change with decreasing proximity to the glaciers due to the additional suspended particles in the water column.

Hypothesis 2: Regarding the kelp response to increasing temperatures, we expect *A. esculenta* (optimum: 8–9°C; Munda and Lüning 1977) to be better adapted to lower temperatures compared to *S. latissima* (optimum: 10–15°C; Bolton and Lüning 1982).

To assess this, we exposed *A. esculenta* and *S. latissima* to three short-term temperature treatments (3°C, 7°C, and 11°C) and examined changes in their photosynthesis vs. irradiance curves and biochemical composition. We expect to find increasing respiration and photosynthetic rates with higher temperature due to higher enzymatic and metabolic activities and differences in the kelps pigment concentrations and carbon to nitrogen ratio. We hypothesize that the different temperature tolerance ranges of the kelps to rising temperatures, result in a temperature-induced variation of the compensation depth, leading to a shift of the species composition.

Methods

Study region

Kongsfjorden is one of the best-studied Arctic fjord ecosystems (Bischof et al. 2019). It represents a model system to study links between changes in the physical environment

(such as glacial retreat) and their effects on ecological processes, which serve as indicators for future Arctic conditions (Bischof et al. 2019). It is located at 79°N at the west coast of Spitsbergen, Norway, being orientated from southeast to northwest. It is about 20 km long (Fig. 1) and up to 350 m deep. Its tidal range is about 0.5 m. Since 2014, SSTs between -1.8°C in winter and $+8.35^{\circ}\text{C}$ in summer were recorded (AWI-Dashboard, <https://dashboard.awi.de/?dashboard=2847>; 15 July 2022). The fjord is characterized by areas being influenced by different stages of glacial retreat: (1) Three sea-terminating glaciers (Kongsvegen, Kronebreen, Kongsbreen) terminate into the fjord at the southeast coast. (2) Brøggerbreen is a land-terminating glacier on the southern coast, discharging melt water into the Bayelva river and the fjord (Svendsen et al. 2002). (3) In the outer fjord region glacial freshwater release is not in close spatial proximity and relatively clear coastal water prevails, depicting the last stage of glacial retreat.

Underwater light climate measurements and water samples

The spectrally resolved downwelling irradiance was measured (RAMSES-ACC-UV/VIS radiometer; TriOS Optical Sensor) from 400 to 700 nm in July 2021 at 17 depth profiles (Fig. 1; Table S1). At each depth profile, 14 spectral measurements in water depths from 0 to 12.5 m were taken (alternative calibration). All depth profiles were taken between midday and early afternoon (highest light intensities) and only on days with stable and constant light conditions to ensure comparability between the measurements. In each area, we measured several depth profiles: Depth profiles A–J represent the sea-terminating glacier fjord area (zone 3 and 4 after Hop et al. 2002). Depth profiles K–O (zone 3 after Hop et al. 2002) are within the land-terminating fjord area. The coastal

water is represented by depth profiles Q and P (zone 2 after Hop et al. 2002). We measured as many depth profiles as possible under the prevailing environmental conditions to ensure the coverage of a large area in the meltwater plume at the highest possible resolution (sea-terminating glacier: 10, land-terminating glacier: 5, coastal water: 2). Due to the presence of ice bergs during July 2021, we were not able to conduct light measurements closer to the sea-terminating glacier than depth profile A. The irradiance of each wavelength was measured in $\text{mW m}^{-2} \text{nm}^{-1}$ and converted to $\mu\text{mol photons m}^{-2} \text{s}^{-1}$ after Eq. 1.

$$I_{\lambda} = [\lambda(\text{m}) \times X_{\lambda}(\text{Wm}^{-2})] \times [h(\text{Js}) \times c(\text{ms}^{-2}) \times N_A(\text{mol}^{-1})]^{-1} = \mu \text{ mol photons m}^{-2} \text{ s}^{-1} \quad (1)$$

PAR was calculated by integrating the irradiance (I_{λ}) from 400 to 700 nm (Eq. 2). As the downwelling irradiance was measured every 2.1 nm, PAR values were corrected by this factor in consultation with the manufacturer.

$$I_{\text{PAR}} = \int_{400}^{700} I_{\lambda} d\lambda \times 2.1 = \sum_{400}^{700} I_{\lambda} \times 2.1 = \mu \text{ mol photons m}^{-2} \text{ s}^{-1} \quad (2)$$

Based on these calculations, the Kongsfjorden underwater light climate in July 2021 was modeled using Ocean Data View, version 5.5.1 (Schlitzer 2021). The model (DIVA gridding, X scale-length: 40 permille, Y scale-length: 30 permille) shows the \log_{10} of PAR irradiances to highlight low irradiances, which are relevant for the kelp's lower depth limit. The kelps compensation depth was based on the measured compensation irradiance

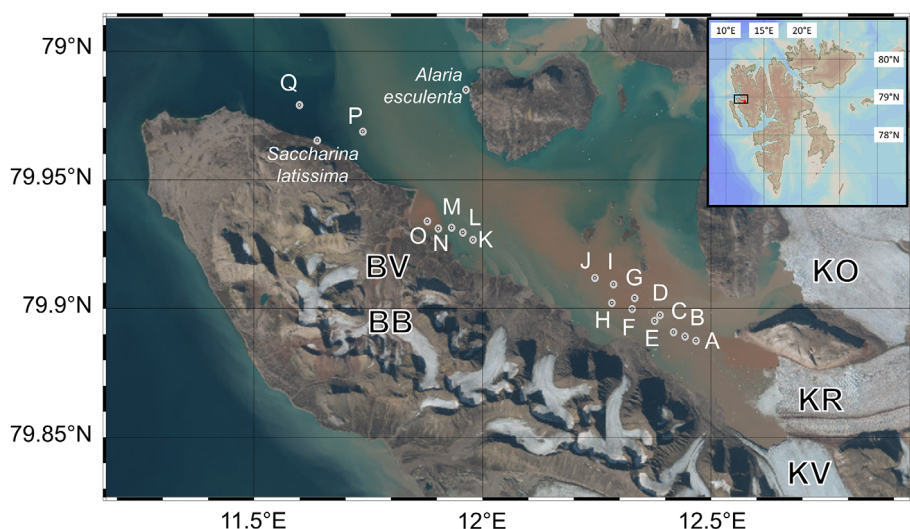


Fig. 1. Sampling sites in Kongsfjorden, Svalbard. Positions of the underwater light climate depth profiles (A–Q) and kelp sampling sites (*Saccharina latissima*, *Alaria esculenta*) in Kongsfjorden, Svalbard. Right upper corner: Overview map of Svalbard; black rectangle marks the position of Kongsfjorden. BB: Brøggerbreen; BV: Bayelva river; KV: Kongsvegen; KR: Kronebreen; KO: Kongsbreen. Brownish water: high concentrations of suspended particles in the water. Map: Ocean Data View (Schlitzer 2021). Satellite image: <https://toposvalbard.npolar.no/>; 15 July 2022.

(see paragraph below). It was calculated by fitting a linear function on the \log_{10} -PAR irradiance measurements of each depth profile. The mean compensation irradiance of each species and temperature was inserted into the linear function and the equation was solved for the water depth.

The depth profile's spectrum peak describes the wavelength with the maximum irradiance transmission through the water column. It was calculated as the average over the spectral measurements in depth (0–12.5 m) (Eq. 3) and is used as proxy to quantify the overlap of the underwater light climate with the pigment absorption (Wondraczek et al. 2013).

$$\lambda(\text{depth profile's spectrum peak}) = \bar{X}(\max I_{\lambda}(0\text{m}); \max I_{\lambda}(0.5\text{m}); \dots; \max I_{\lambda}(12.5\text{m})) = \text{nm} \quad (3)$$

At each depth profile, a surface water sample was taken to determine the salinity with a refractometer.

Kelp sampling and temperature experiment

Scientific SCUBA divers collected *S. latissima* and *A. esculenta* sporophytes in Kongsfjorden, Svalbard from 6 to 9 m depth (Fig. 1; Table S1). Sporophytes of the same species were of similar size. Meristematic discs (diameter = 2 cm) were cut and distributed between temperature treatments and replicates ($n = 4$), avoiding pseudo-replication. They were cultivated in 1 L aerated glass beakers, filled with filtered seawater (changed every 2 d), applying 24 h of constant light ($24 \mu\text{mol photons m}^{-2} \text{s}^{-1}$). The experiment ran for 7 d ($t_0 - t_7$), with temperature treatments of 3°C (in situ SST; July 2021, 10 m depth), 7°C (present high SSTs; AWI-Dashboard, <https://dashboard.awi.de/?dashboard=2847>; 15 July 2022) and 11°C (future SST by the year 2100; Skogseth et al. 2020). Treatment temperature was increased every 2 d by 4°C, allowing for successive acclimation (Fig. 2). After photosynthesis vs. irradiance curves were measured on t_3 , t_5 , and t_7 , the samples were silica-dried and stored in darkness until biochemical analysis.

Kelp response parameters

To quantify the kelp response to rising temperatures, we measured photosynthetic vs. irradiance curves, the maximum quantum yield of photosystem II (F_v/F_m), pigment concentrations and carbon to nitrogen ratio. Photosynthetic vs. irradiance curves were measured on t_3 , t_5 , and t_7 (Fig. 2) to measure whether increasing temperature changes the kelp light-use characteristics. Therefore, we measured the oxygen concentration evolution under different light intensities, using an optode set-up of PyroScience. Dark respiration and net photosynthetic rates were calculated in $\mu\text{mol O}_2 \text{L}^{-1} \text{cm}^{-2} \text{h}^{-1}$. Subsequently, we analyzed F_v/F_m with a chlorophyll fluorometer of dark-adapted discs, which is used as proxy to quantify algal cellular and physiological stress level. As the algal pigment composition is crucial to absorb light for photosynthesis, we analyzed the chlorophyll *a* (Chl *a*)

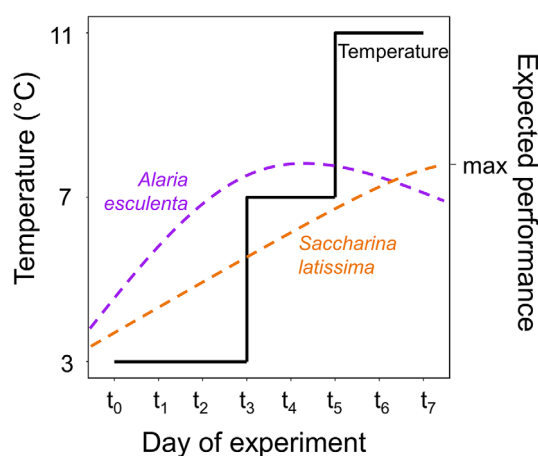


Fig. 2. Experimental set-up. The treatments temperature (°C) (solid black line) was increased by 4°C on t_3 and t_5 of the experiment until the treatment's temperature was reached (3°C, 7°C, and 11°C). Photosynthesis vs. irradiance curve were measured on t_3 (3°C treatment), t_5 (7°C treatment), and t_7 (11°C treatment). Dashed purple line: expected performance of *Alaria esculenta* based on Munda and Lüning (1977). Dashed orange line: expected performance of *Saccharina latissima* based on Bolton and Lüning (1982).

concentration and ratio of accessory pigments to Chl *a* after Koch et al. (2015) and Wright et al. (1991). Pigment contents were calculated in $\mu\text{g cm}^{-2}$. Furthermore, we quantified the kelps carbon to nitrogen ratio, to analyze for temperature-induced carbon gain or loss (photosynthesis and respiration). We measured the carbon to nitrogen ratio by combustion of dried kelp material and using Acetanilide as standard (Verardo et al. 1990). Total carbon and nitrogen content were expressed as proportion (%) and ratio. *A. esculenta* and *S. latissima* are morphologically different, with the meristematic discs of *S. latissima* being ~85% heavier (fresh weight; data not shown) than *A. esculenta*. To be able to compare the temperature-induced responses, we standardized all parameters to the discs total area (cm^2), including the front- and backside of the discs.

A detailed description of all methods to measure the kelp response parameters can be found as Supporting Information.

Statistics

All statistical analyses of the physiological and biochemical data were run in RStudio (Version 2021.09.0 + 351; R Core Team 2021). A linear model was fit on the data of each parameter, using the “lm” function of the R package “stats”. Species (*S. latissima*, *A. esculenta*) and treatment's temperature (3°C, 7°C, 11°C) were modeled as multiple fixed effects. For the analysis of the compensation depth and spectrum peak, the fixed effect of area (sea-terminating glacier; land-terminating glacier; coastal water) was included. Each model's fit on the data was assessed by evaluating the Akaike information criterion and Bayesian information criterion. The normality (Shapiro–Wilk test, $p > 0.05$) and homoscedasticity (Levene's test, $p > 0.05$) of the model's residuals were tested. Analysis of

variance was tested on the model by using the “anova” function, to assess the influence of the fixed effects. Pairwise comparisons were performed, using the “emmeans” function of the R package “emmeans” (Lenth 2021), to calculate the degrees of freedom and Tukey adjustment of the *p* value. Linear dependency of the response variables was determined by calculating the Pearson correlation coefficient, using the “cor.test” function of the R package “stats” (R Core Team 2021) after testing for normality (Shapiro–Wilk test, *p* > 0.05).

Results

Underwater light climate

Comparing the aerial view of Kongsfjorden, distinct melt-water plumes of the sea- and land-terminating glaciers are

clearly visible. The brown, sediment-rich water is contrasting the blue, clear water (Fig. 1).

PAR intensities and kelp compensation depth

The modeled PAR intensities of Kongsfjorden in different water depths can be seen in Fig. 3a,b. PAR intensities over depth varied strongly between the three fjord regions. Depth profile Q (coastal water) was characterized by the highest PAR intensities. On 12.5 m, PAR intensities of 81 $\mu\text{mol photons m}^{-2} \text{s}^{-1}$ were measured, while in depth profile A (sea-terminating glacier) the lowest PAR intensity was measured ($\sim 0.01 \mu\text{mol photons m}^{-2} \text{s}^{-1}$). Comparing the mean PAR intensities of all areas on 4.5 m, it was highest in the coastal water and lowest near the land-terminating glacier (coastal water: $254.7 \pm 24.55 \mu\text{mol photons m}^{-2} \text{s}^{-1}$ > sea-terminating glacier: $24.8 \pm 30.53 \mu\text{mol photons m}^{-2} \text{s}^{-1}$ > land-terminating glacier: $8.5 \pm 5.58 \mu\text{mol photons m}^{-2} \text{s}^{-1}$). The

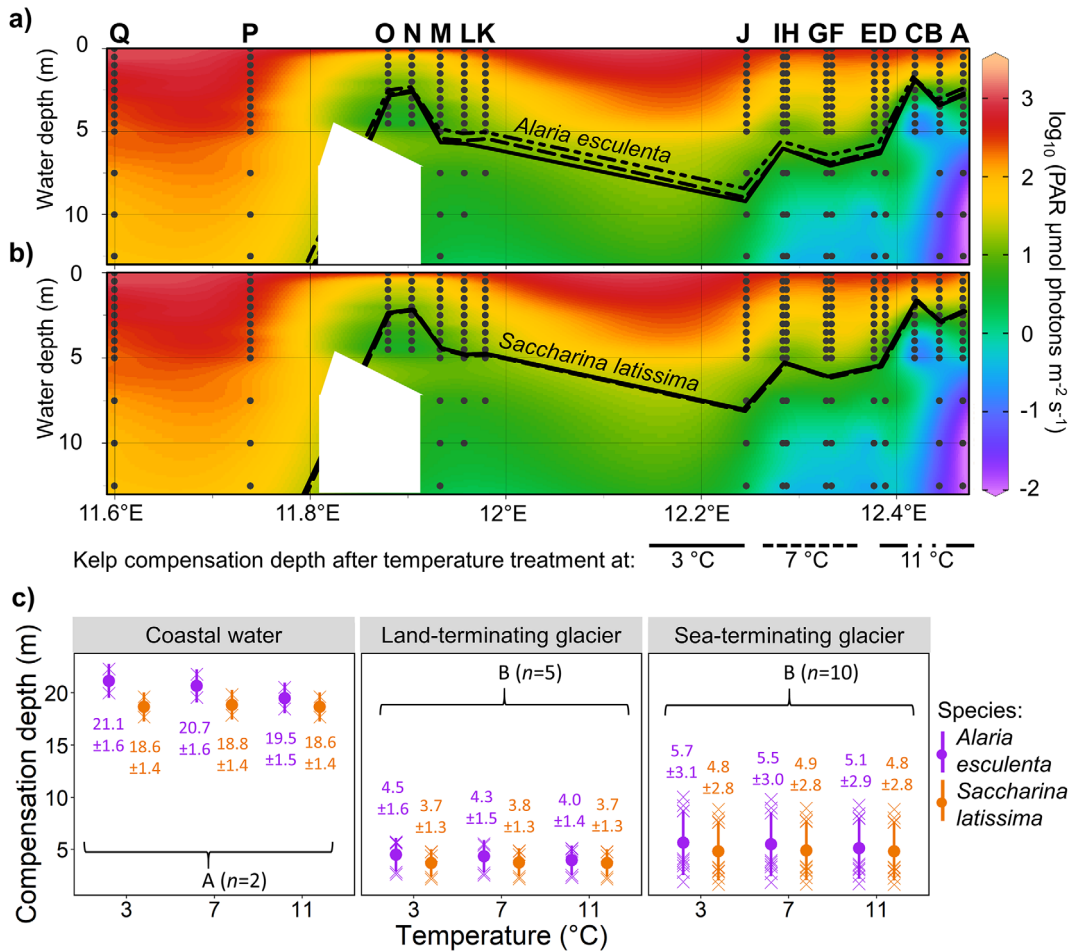


Fig. 3. Photosynthetically active radiation (PAR) in Kongsfjorden, Svalbard. Model of the underwater light climate (log₁₀ of PAR irradiances; 400–700 nm) along a longitudinal section through Kongsfjorden, covering all depth profiles (A–Q) and water depths (0–12.5 m). Depth profile P, Q: coastal water. Depth profile O–K: influence of land-terminating glacier. Depth profile A–J: influence of sea-terminating glaciers. Black dots: spectral measurements. White area: insufficient data coverage for model. Black lines in the plots: compensation depth of (a) *Alaria esculenta* and (b) *Saccharina latissima* being cultivated at 3°C (solid line), 7°C (dashed line) and 11°C (dash-dot-dot line). (c) Compensation depth of both species (*A. esculenta*: purple, *S. latissima*: orange) in all fjord areas (coastal water, land-terminating glacier, sea-terminating glacier) after different temperature treatments (3°C, 7°C, 11°C). Temperature mean (dot) ± SD (number associated to each point) and depth profile response (cross). Different capital letters indicate significant differences between area, temperature, and species.

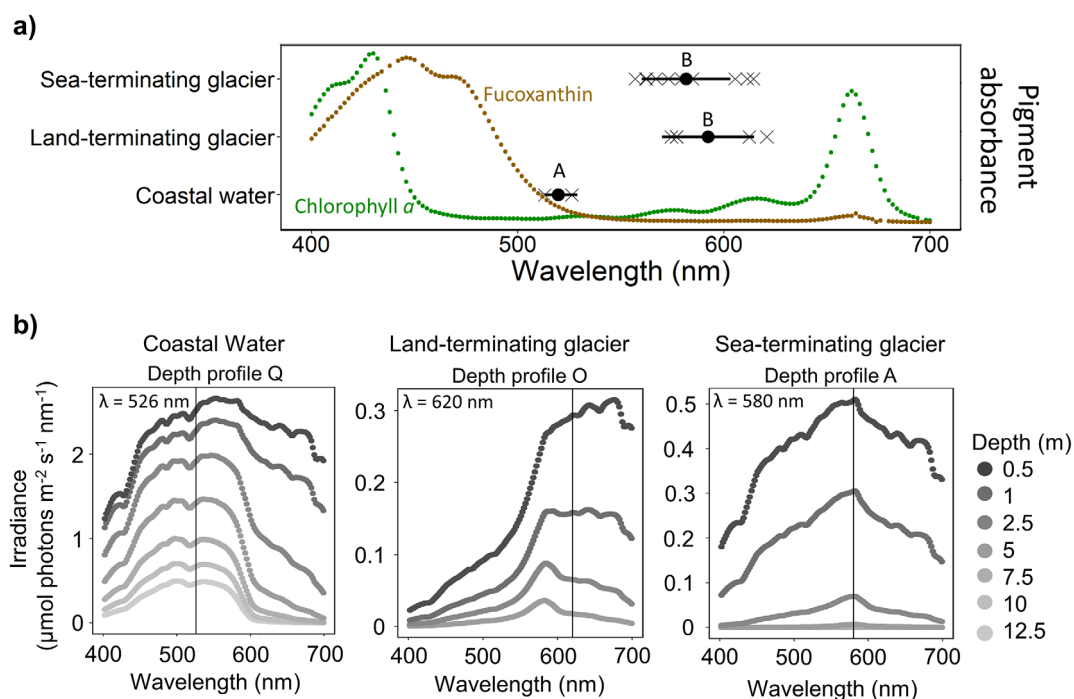


Fig. 4. Spectrum peaks. **(a)** Spectrum peaks (wavelength with the highest light transmission through the water column) of the three fjord areas (sea-terminating glacier, land-terminating glacier, coastal water). Area mean (black dots) \pm SD and depth profile spectrum peak (black cross) ($n = 2-10$). Different capital letters indicate significant differences between areas. Schematic light absorption curve of chlorophyll *a* (green line) and fucoxanthin (brown line) after Jeffrey et al. (1997). **(b)** Spectrally resolved underwater light climate of different water depths of depth profile Q, O, and A. Vertical black line; λ : depth profiles spectrum peak. Note the different y-axis scales of the subplots.

compensation depth for *A. esculenta* (Fig. 3a) and *S. latissima* (Fig. 3b) was modeled based on the measured compensation irradiance (see paragraph below) and follows the variations in PAR intensities. While we detected no significant changes in the compensation depth between species ($p = 0.163$; $F_{1,84} = 1.985$) or temperature ($p = 0.841$; $F_{2,84} = 0.174$), the fjord area showed significant differences ($p < 0.001$; $F_{2,84} = 188.536$). The compensation depths of both species were significantly higher in the coastal area compared to the glacier-influenced areas (Fig. 3c). In the coastal water, the potential compensation depth for both kelp species and all temperature treatments was below 17 m. Furthermore, we detected three trends (Fig. 3): (1) With increasing temperature, the compensation depth of *A. esculenta* shifts to shallower water depths by a mean of $10.4 \pm 0.2\%$ independently of the fjord region. *S. latissima* showed no temperature dependent differences. (2) The compensation depth of *S. latissima* is $11.3 \pm 0.05\%$ shallower compared to *A. esculenta*. (3) Within the glacial areas, the compensation depth of both species increases with increasing distance to the glacier front.

Spectral composition

The spectral characteristics of the underwater light climate in different water depths of each area are shown in Fig. 4. The mean spectrum peak of the areas varied significantly ($p = 0.0032$; $F_{2,14} = 8.925$), with spectrum peak of the coastal water area (519.72 ± 9.30 nm) being significantly lower

compared to the mean spectrum peak of the land-terminating glacier (592.34 ± 22.31 nm, $p = 0.0028$) and sea-terminating glacier (581.70 ± 21.50 nm; $p = 0.0053$) area (Fig. 4a). While the mean spectrum peak of all three areas are within the green gap of Chl *a*, the spectrum peaks of the coastal area are close to the absorption of fucoxanthin. The spectrum peaks of the areas being influenced by glaciers are out of the spectral absorption range of fucoxanthin. Comparing the spectral light composition of depth profiles for each fjord region (coastal water: depth profile Q; land-terminating glacier: depth profile O; sea-terminating glacier: depth profile A), three characteristics can be seen (Fig. 4b): (1) in all fjord regions, the irradiance of each wavelength is decreasing with increasing water depth. (2) Comparing the same water depth, the irradiance is highest in the outer fjord region (depth profile Q) and lowest near the Bayelva river mouth (depth profile O) and (3) not only the depth profiles spectrum peak is shifting, but the whole spectral composition is changing.

Salinity

The water's surface salinity (S_A) varied significantly between all areas ($p < 0.001$; $F_{2,48} = 11.704$). The coastal water had the highest mean salinity ($S_A = 36.75 \pm 0.82$), followed by the surface salinity of the land-terminating glacier area ($S_A = 27.80 \pm 3.16$) and the sea-terminating glacier area ($S_A = 31.15 \pm 4.46$), which were significantly lower. Within

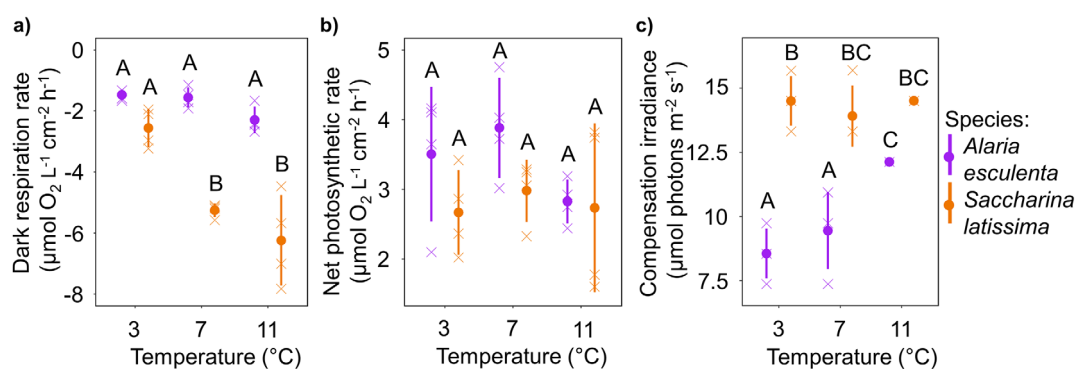


Fig. 5. Respiration and photosynthesis. Photosynthetic responses of *Alaria esculenta* (purple) and *Saccharina latissima* (orange) after different temperature treatments (3°C, 7°C, and 11°C). Treatment mean (dots) \pm SD and average replicate response (cross) ($n = 3-4$). Different capital letters indicate significant ($p < 0.05$) differences between the temperature treatments and species. **(a)** Dark respiration rate ($\mu\text{mol O}_2 \text{ L}^{-1} \text{ cm}^{-2} \text{ h}^{-1}$). **(b)** Net photosynthetic rate ($\mu\text{mol O}_2 \text{ L}^{-1} \text{ cm}^{-2} \text{ h}^{-1}$). **(c)** Compensation irradiance ($\mu\text{mol photons m}^{-2} \text{ s}^{-1}$). Some error bars are within the diameter of the symbol.

the land-terminating glacier area, the salinity was lowest of depth profile O ($S_A = 26$), showing an increasing trend with increasing distance to the Bayelva river mouth ($S_A = O < N < L < K$). The salinity of the sea-terminating glaciers influenced depth profiles A-J, showed no clear spatial trend.

Kelp response parameters

Dark respiration rate

The dark respiration rate ($\mu\text{mol O}_2 \text{ L}^{-1} \text{ cm}^{-2} \text{ h}^{-1}$) was significantly affected by species ($p < 0.001$; $F_{1,18} = 102.675$) and temperature ($p < 0.001$; $F_{2,18} = 20.96$), as well as their interaction ($S \times T$) ($p = 0.001$; $F_{2,18} = 10.12$; Fig. 5a). After all temperature treatments, the mean dark respiration rate of *A. esculenta* was between 42% and 71% lower than of *S. latissima*. With increasing temperature, the dark respiration rate of *S. latissima* increased (decreasing oxygen concentrations) significantly ($[11^\circ\text{C} = 7^\circ\text{C}] > [3^\circ\text{C}]$), while the dark respiration rate of *A. esculenta* only showed an increasing trend.

Net photosynthetic rate

The net photosynthetic rate ($\mu\text{mol O}_2 \text{ L}^{-1} \text{ cm}^{-2} \text{ h}^{-1}$) was neither significantly affected by species ($p = 0.069$; $F_{1,18} = 3.741$), temperature ($p = 0.268$; $F_{2,18} = 1.417$) nor their interaction ($p = 0.519$; $F_{2,18} = 0.681$; Fig. 5b), being $3.1 \pm 0.48 \mu\text{mol O}_2 \text{ L}^{-1} \text{ cm}^{-2} \text{ h}^{-1}$ on average for both species and temperatures. No significant temperature-induced response was observed. Although the mean net photosynthetic rate of *A. esculenta* was highest after the 7°C treatment, the difference was not significant due to the high variability in the replicates response.

Compensation irradiance

Species ($p < 0.001$; $F_{1,17} = 106.158$), temperature ($p = 0.003$; $F_{2,17} = 8.579$), and their interaction ($p = 0.010$; $F_{2,17} = 6.042$) had a significant effect on the compensation irradiance ($\mu\text{mol photons m}^{-2} \text{ s}^{-1}$) (Fig. 5c). Independently of the temperature, the mean compensation irradiance of *A. esculenta* was lower

compared to *S. latissima*, being 41% lower after the 3°C treatment. The compensation irradiance of *A. esculenta* increased significantly by 29% with increasing temperature, while the compensation irradiance of *S. latissima* showed no temperature-induced response, being $14.3 \pm 0.35 \mu\text{mol photons m}^{-2} \text{ s}^{-1}$ after all temperature treatments.

F_v/F_m

Mean F_v/F_m values of all species and temperature treatments were between 0.72 and 0.76. F_v/F_m was significantly affected by species ($p < 0.001$; $F_{1,18} = 15.219$) and temperature ($p < 0.001$; $F_{2,18} = 13.029$), while their interaction ($p = 0.183$; $F_{1,18} = 1.869$) had no significant effect (Table 1). With increasing temperature, F_v/F_m of *A. esculenta* and *S. latissima* increased significantly.

Chlorophyll a

Species ($p < 0.001$; $F_{1,18} = 250.027$) and temperature ($p = 0.01$; $F_{2,18} = 6.088$) had a significant effect on Chl a concentration ($\mu\text{g cm}^{-2}$) ($p < 0.05$), while their interaction ($p = 0.191$; $F_{2,18} = 1.8148$) had no effect (Table 1). Independently of the temperature, the Chl a concentration of *A. esculenta* was $\sim 78\%$ higher than the Chl a concentration of *S. latissima*. Chl a of both species was highest after the 11°C treatment, being only significant for *A. esculenta*.

Accessory pigments to Chl a ratio

The ratio of accessory pigments to Chl a was neither significantly affected by species ($p = 0.581$; $F_{1,18} = 0.318$), temperature ($p = 0.235$; $F_{2,18} = 1.589$), nor their interaction ($p = 0.741$; $F_{2,18} = 0.306$; Table 1). No significant differences between *A. esculenta* or *S. latissima* were detected after the temperature treatments.

Carbon

The total carbon content (%) was significantly influenced by species ($p < 0.001$; $F_{1,18} = 96.766$) and the interaction of species and temperature ($p = 0.015$; $F_{2,18} = 5.334$), while the temperature alone had no significant effect ($p = 0.350$; $F_{2,18} = 1.113$;

Table 1. Kelp response parameters. Maximum quantum yield of photosystem II (F_v/F_m), chlorophyll a ($\mu\text{g cm}^{-2}$), ratio of accessory pigments to chlorophyll a , total carbon content (%), total nitrogen content (%) and carbon to nitrogen ratio of *Alaria esculenta* and *Saccharina latissima* after different temperature treatments (Temp.). Different capital letters indicate significant (Sig.; $p < 0.05$) differences between the temperature treatments and species within one parameter.

Parameter	Temp.	<i>Alaria esculenta</i>			<i>Saccharina latissima</i>		
		Mean	\pm SD	Sig.	Sig.	Mean	\pm SD
F_v/F_m	3°C	0.72	0.011	A	B	0.741	0.015
	7°C	0.749	0.011	BC	BC	0.754	0.007
	11°C	0.742	0.004	BC	C	0.764	0.006
Chlorophyll a ($\mu\text{g cm}^{-2}$)	3°C	7.81	1.45	AC	B	1.66	1.1
	7°C	7.56	1.25	A	B	1.64	0.095
	11°C	10.1	1.14	C	B	2.36	0.295
Accessory pigments to chlorophyll a ratio	3°C	0.216	0.025	A	A	0.222	0.012
	7°C	0.213	0.008	A	A	0.207	0.026
	11°C	0.204	0.025	A	A	0.193	0.023
Carbon content (%)	3°C	37.0	1.36	A	B	32.4	2.17
	7°C	37.9	2.09	A	BC	29.6	1.64
	11°C	38.8	2.66	A	C	27.6	1.86
Nitrogen content (%)	3°C	1.27	0.112	A	A	1.36	0.226
	7°C	1.34	0.316	A	A	1.18	0.104
	11°C	1.55	0.324	A	A	1.23	0.326
Carbon to nitrogen ratio	3°C	29.5	3.69	A	A	24.2	3.09
	7°C	29.4	6.81	A	A	25.3	3.47
	11°C	26.3	8.49	A	A	23.5	5.95

F_v/F_m , chlorophyll a , ratio of accessory pigments to chlorophyll a , total carbon and nitrogen content, and carbon to nitrogen ratio were tested against the single and interactive effects of species and temperature. Values are the treatment means ($n = 4$) \pm SD.

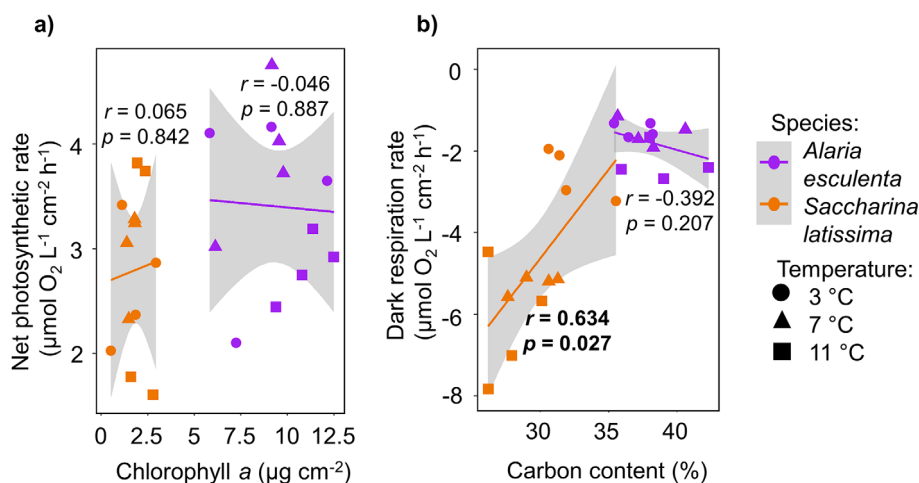


Fig. 6. Correlations. Linear dependency between two response parameters of *Alaria esculenta* (purple) and *Saccharina latissima* (orange) after different temperature treatments (circle: 3°C, triangle: 7°C; box: 11°C; $n = 3-4$). Gray area: 95% confidence interval. r : Pearson correlation coefficient. Significant correlations ($p < 0.05$) are marked in bold. (a) Net photosynthetic rate ($\mu\text{mol O}_2 \text{ L}^{-1} \text{ cm}^{-2} \text{ h}^{-1}$) vs. chlorophyll a content ($\mu\text{g cm}^{-2}$). (b) Dark respiration rate ($\mu\text{mol O}_2 \text{ L}^{-1} \text{ cm}^{-2} \text{ h}^{-1}$) vs. total carbon content (%).

Table 1). The mean carbon content of *A. esculenta* was 12–29% higher than of *S. latissima*. The carbon content of *S. latissima* decreased significantly with increasing temperature, while the carbon content of *A. esculenta* showed an increasing trend with increasing temperature.

Nitrogen

The total nitrogen content (%) was not significantly affected by the tested fixed effects (species: $p = 0.223$; $F_{1,18} = 1.591$; temperature: $p = 0.599$; $F_{2,18} = 0.527$; interaction: $p = 0.289$; $F_{2,18} = 1.333$; Table 1). No significant

differences between *A. esculenta* and *S. latissima* were detected after the temperature treatments.

Carbon to nitrogen ratio

The carbon to nitrogen ratio was not affected by the tested fixed effects (species: $p = 0.094$; $F_{1,18} = 3.127$; temperature: $p = 0.669$; $F_{2,18} = 0.411$; interaction: $p = 0.906$; $F_{2,18} = 0.099$; Table 1). The mean carbon to nitrogen ratio was 26.37 ± 2.57 for both species after all temperature treatments, showing no significant changes.

Correlations

In both species, the photosynthetic rate did not correlate significantly with the Chl *a* concentration (*A. esculenta*: $p = 0.887$, $t = -0.146$, $df = 10$; *S. latissima*: $p = 0.842$, $t = 0.205$, $df = 10$; Fig. 6a). The carbon content of *S. latissima* decreased significantly with increasing respiration rate ($p = 0.027$, $t = 2.591$, $df = 10$). In *A. esculenta* the correlation was not significant ($p = 0.207$, $t = -1.350$, $df = 10$) (Fig. 6b).

Discussion

Kelps act as important foundation species in Arctic rocky shore ecosystems (Filbee-Dexter et al. 2019). Currently, they are experiencing major changes in their habitat's environment. According to Constable et al. (2022), the SST in Arctic regions is predicted to increase drastically by the end of the century. At a warming rate of 0.7°C per decade, a mean summer SST of 11°C will be reached in ~ 100 years (Skogseth et al. 2020), although extreme temperature events will reach 11°C earlier. While the Arctic endemic marine vegetation is likely to be lost (Bringloe et al. 2020), a poleward expansion of temperate kelp species is projected (Krause-Jensen et al. 2020; Assis et al. 2022). However, with rising SSTs, terrestrial run-off is also increasing (Constable et al. 2022), which was shown to deteriorate the underwater light climate (Konik et al. 2021), impeding net photosynthesis and, hence, result in a shift of the kelp forest to shallower waters (Filbee-Dexter et al. 2019). Our study aimed to address two critical aspects related to Arctic kelp ecophysiology: the characterization of the underwater light climate at different stages of glacial retreat and the response of Arctic kelp species (*A. esculenta*, *S. latissima*) to different light and thermal conditions. **We found a strong spatial variation in the underwater light climate within Kongsfjorden, with the light intensity being reduced and the spectral composition shifting toward longer wavelengths near glaciers. That significantly affected the kelp compensation depth, leading to a shoaling of the kelp forest near glaciers** (Hypothesis 1). Our results further showed that rising SSTs are affecting kelp light-use characteristics, with *A. esculenta* being better adapted to polar conditions than *S. latissima*. These differences in the responses might result in a future shift in species composition (Hypothesis 2).

Variation of the underwater light climate due to glacial retreat

With ongoing climate change, glaciers were shown to retreat (Hugonnet et al. 2021). Geyman et al. (2022) found that the glacier mass loss is predicted to double until 2100, compared to the 20th century. Concomitantly, species distribution models estimate a current potential distribution of kelp forests in the Arctic of $655,000 \text{ km}^2$ (Assis et al. 2022), potentially being influenced by glaciers and glacial run-off.

Comparing the underwater light climate of all three fjord areas, we observed distinct differences. Near glaciers (depth profile O, A), the reduction of PAR was much stronger, compared to the clearer water at the outside of the fjord (Fig. 3a,b). This can be explained by the high concentration of suspended particles of the meltwater plumes, which additionally absorb and scatter the available light (Stomp et al. 2007). Hence, high meltwater run-off rates (and consequently sediment concentrations in the water) resultant from retreating glaciers lead to less available light for photosynthesis (Payne and Roesler 2019).

Additional to the PAR intensity, we analyzed the spectral composition of the downwelling irradiance and compared its overlap with the light absorption spectrum of Chl *a* and fucoxanthin (Fig. 4a). The main absorption peaks of Chl *a* are at 430 nm (blue light) and 662 nm (red light), leaving a major green gap in which light absorption is low (Jeffrey et al. 1997). Fucoxanthin and chlorophyll *c*, belonging to the major accessory pigments of brown algae, close this green gap partly, as their main absorption peaks are between 445 and 468 nm (blue light) (Jeffrey et al. 1997). We found that all spectrum peaks (wavelength with the highest light transmission through the water column) were within the green gap of Chl *a* (Fig. 4a). However, the spectrum peaks of coastal water were close to the absorption spectrum of fucoxanthin, resulting in a large overlap of the light spectrum with the pigment absorption spectrum. The spectrum peaks of the glacier-influenced depth profiles were well outside the absorption range of fucoxanthin, leading to a very limited overlap of the spectra. The photosynthetic efficiency is dependent on the overlap between the prevailing light spectrum and the absorption spectrum of the pigments (Wondraczek et al. 2013). Therefore, high meltwater rates and sediment concentrations reduce the quality of the downwelling irradiance for photosynthesis and biomass accumulation of kelps. Loos et al. (2017) described significant variations of the spectral composition, depending on the distance to a river mouth, being correlated to the concentration of suspended particles in the water column. Furthermore, a similar shift of the spectrum was described by Stomp et al. (2007), who compared the spectral niches in the water column and their availability for photosynthetic organisms of clear ocean, coastal water, and a peat lake.

Comparing the underwater light climate of all three areas, the variation of the PAR intensities translated into a significant difference in the kelp's compensation depth, showing

that an increased run-off results in a shift of the lower depth limit to shallower waters. We found the lowest light intensities and strongest change of the spectral composition near the land-terminating glacier. However, it has to be considered that the distance of depth profile O (closest to land-terminating glacier) to the Bayelva river mouth is much smaller than the distance of depth profile A (closest to sea-terminating glacier) to the sea-terminating glacier front (Fig. 1). In addition, the sediment plume of sea-terminating glaciers was much more pronounced, influencing a larger area of the fjord (Fig. 1). Sediment plumes of land-terminating glacier were influenced by wind direction and currents to a higher degree (pers. obs.).

Therefore, we conclude that the darkening of the water column as well as the change of the spectral composition of the light in the Arctic may lead to a reduction of the available habitat for kelp forests near retreating glaciers. We also found that the strong negative influence of melting sea-terminating glaciers on the underwater light climate may reduce as they become land-terminating.

Kelp responses to rising SST

Metabolic processes depend on enzymatic reactions (Davison et al. 1991) and are characterized by the integration of different intrinsic enzymatic properties. Therefore, metabolic pathways have a temperature optimum at which they are at their maximal capacity (Daniel et al. 2008). Currently, many kelps species are experiencing temperatures below their optimum in the Arctic (Krause-Jensen et al. 2020). Above or below the temperature optimum, the physiological stress increases (Pörtner et al. 2005), leading to smaller kelp individuals in the Arctic compared to mid-latitude range populations (Borum et al. 2002). As proxy for algal cellular and physiological stress level (Murchie and Lawson 2013), we assessed F_v/F_m after all temperature treatments. Despite significant changes of F_v/F_m between species and temperature treatments, all recorded values were > 0.7 (Table 1), which is considered healthy for kelps (Dring et al. 1996). Therefore, no damaging effect on photosystem II occurred during our experiment and the electron transfer was not impaired (Li et al. 2017). Hence, we conclude that the temperature increase during the experiment did not have negative effects on the performance of the kelps.

Nevertheless, we found significant species-specific differences in the temperature responses, depicting a different effect of increasing SSTs on their balance of carbon uptake and loss. The dark respiration rates of *A. esculenta* were lower compared to *S. latissima* after all temperature treatments. While it was significantly lower after the 7°C and 11°C treatment, we detected no significant difference after the 3°C treatment, when the respiration rate of *S. latissima* was comparably low to *A. esculenta*. We interpret the low respiration rate of *S. latissima* at 3°C as a limitation of enzymatic capacities, reducing potential respiration rates (Atkin and Tjoelker 2003). The high dark respiration rates of *S. latissima* at 7°C and 11°C indicate a higher mitochondrial adenosine triphosphate

formation capacity (Pörtner et al. 2005) and therefore more cellular energy. However, we also observed a significant correlation between the increasing dark respiration rates and decreasing carbon content in *S. latissima* (Fig. 6b). As the carbon to nitrogen ratio was determined after the photosynthesis vs. irradiance curves were measured, we conclude that the low carbon content depicts the carbon loss during dark respiration (Saltveit 2019). Neither the dark respiration rate nor the total carbon content of *A. esculenta* did change significantly with higher temperatures (Fig. 5a; Table 1). The carbon content displays kelp storage compounds, such as Mannitol and Laminarin (Scheschonk et al. 2019). Mannitol was shown to be crucial in cellular osmotic regulation, cell turgor control and freezing protection (Iwamoto and Shiraiwa 2005; Elliott et al. 2017) and is converted into the long-term carbon-storage product laminarin (Graiff et al. 2016; Scheschonk et al. 2019). We hypothesize that the high carbon content of *A. esculenta*, enables it to respond to freezing temperatures and salinity fluctuations, which we also observed in Kongsfjorden. Furthermore, the low dark respiration rates of *A. esculenta* prevents carbon loss during dark periods, enabling it to maintain a higher degree of growth and performance (Davison et al. 1991). This confirmed our expectation that *A. esculenta* is better adapted to low temperatures than *S. latissima* (optimal growth temperatures after Munda and Lüning 1977 and Bolton and Lüning 1982). Thereby, it is noteworthy to mention that the optimum temperatures, described for temperate populations, hold also true for Arctic populations. Evidence of a high overall resilience toward low temperatures of *A. esculenta* was reported by Bringloe et al. (2022), showing that *A. esculenta* populations were resilient to past glaciation events and adapted to Arctic conditions.

Based on the low respiration rates of *A. esculenta* during the entire experiment (low carbon loss), we expected that *A. esculenta* would also have higher photosynthetic rates (i.e., higher carbon gain) compared to *S. latissima* (higher performance). However, we detected neither a significant difference between species nor temperature treatments (Fig. 5b). As the net photosynthetic rates were measured at low light conditions ($24 \mu\text{mol photons m}^{-2} \text{s}^{-1}$), we conclude that the photosynthetic rates of both kelp species were restricted by the available light intensity. This implies that the photosynthetic capacity to gain carbon was not limited by the low SSTs but by the prevailing light climate. Hence, in low light conditions, the predicted increasing enzyme activities due to rising temperatures are not causing a higher photosynthetic rate in *A. esculenta* and *S. latissima*.

Considering this, it is striking that the concentration of Chl *a* per area in *A. esculenta* was 78% higher compared to *S. latissima*, as higher Chl *a* concentration indicates higher potential photosynthetic rates. A similar difference in the Chl *a* concentration between both species was reported by Gordillo et al. (2006). We do not think that the observed interspecific difference in the Chl *a* concentration is due to a

low-temperature limitation of Chl *a* synthesis as described by Davison et al. (1991), as we detected neither a temperature-induced change in the absolute Chl *a* concentration nor in the ratio of accessory pigments to Chl *a* (Table 1). The high Chl *a* concentrations of *A. esculenta* in combination with the comparably low photosynthetic rates (Fig. 6a) rather indicate a higher amount of inactive photosynthetic reaction centres compared to *S. latissima*. Falkowski and Raven (2007) described a significant reduction of active photosynthetic reaction centres due to low nutrient environments. In summer, water masses in Arctic fjords are characterized by a strong stratification due to temperature and salinity gradients and the absence of vertical mixing (Cottier et al. 2010), resulting in a nutrient depletion (Gordillo et al. 2006). As no extra nutrients were added to the temperature treatments during the experiment, we found the discs to be nitrogen limited, with a carbon to nitrogen ratio between 23 and 30 (Atkinson and Smith 1983). We interpret the distinct difference in Chl *a* concentration between the species (78% higher in *A. esculenta*) as Arctic adaptation of *A. esculenta*, enabling a fast increase of photosynthetic rates with increasing nutrient concentrations.

Additional to temperature-induced alterations in kelp carbon uptake and loss, we found that rising temperatures have the potential to increase the light requirement to balance both processes (compensation irradiance). Relating the measured compensation irradiance of *A. esculenta* and *S. latissima* to the underwater light climate modeled for the three areas in Kongsfjorden (Fig. 3a,b), we found that the overall compensation depth of both species is between ~ 2 and 9 m. This corresponds to SCUBA-based field-surveys by Bartsch et al. (2016) and L. Düsedau pers. comm. Therefore, we consider our results of the compensation irradiance to be accurate. While we did not detect a significant change of the dark respiration rate or the photosynthetic rate of *A. esculenta* with increasing treatment temperature, the compensation irradiance increased significantly. However, the compensation irradiance cannot be derived directly from the dark respiration and photosynthetic rate, as respiration rates of plants in light were shown to vary between 25% and 100% from the dark respiration rates (Krömer 1995). Therefore, we conclude that the ratio of respiration during photosynthesis in light of *A. esculenta* changes with rising SSTs, leading to a higher compensation irradiance. At 3°C and 7°C, we found that the mean compensation irradiance of *A. esculenta* was 30–40% lower compared to *S. latissima*. These results suggest that *A. esculenta* is capable of net photosynthesis in low PAR environments and is therefore better adapted to low underwater light climate and temperatures in Arctic fjords. At low temperatures, its potential habitat is bigger compared to *S. latissima*. However, we also found that the compensation irradiance of *A. esculenta* is highly temperature sensitive. After exceeding the temperature optimum of 8–9°C in the 11°C treatment, the compensation irradiance of *A. esculenta* was significantly higher compared to the 3°C treatment. While our results did not indicate a significant

increase of the compensation irradiance for *S. latissima* (Fig. 5c), Davison et al. (1991) found a significantly higher compensation irradiance with increasing temperature, comparing young *S. latissima* sporophytes being exposed to temperatures from 5°C to 25°C. This shows that rising SSTs have the potential to affect the light requirement necessary to balance respiration by photosynthesis of both kelp species.

Thereby, the significant variations of the light-use characteristics, biochemical and physiological parameters between both kelp species in response to increasing temperature, might lead to a changed balance of interspecific competition in future Arctic kelp forests.

Ecological implications

Bartsch et al. (2016) and L. Düsedau pers. comm. analyzed the long-term development of kelp depth distribution in Kongsfjorden, comparing the kelp forest structure from 1996–1998 to 2012–2014 and 2021. They found an overall shift of the kelp forest to shallower water depths. Furthermore, Filbee-Dexter et al. (2022) found a positive correlation between low light condition in the Canadian Arctic with reduced kelp biomass. Both studies support our results of a decreased compensation depth with increasing influence of the glacial meltwater plume and rising temperature. Thereby, our results indicate that sea-terminating glaciers have a greater influence on the underwater light climate than land-terminating glaciers. Hence, the negative effect of retreating glaciers on the underwater light climate might be reduced when the glacier terminates on land (note that the kelp compensation depth was still significantly lower compared to coastal waters). Only regarding the effect of the underwater light climate, the potential kelp habitat might increase again after glaciers become land-terminating. Payne and Roesler (2019) modeled phytoplankton productivity in relation to glacier type, accounting for differences in the underwater light climate and rising SSTs. Their findings result in a three-stage concept: (1) Productivity increase due to less sea-ice (high PAR intensities); (2) productivity reduction due to higher glacier melt and sediment release (low PAR intensities); (3) productivity increase after land-termination of the glacier, due to less run-off (high PAR intensities). Although the availability of other resources (e.g., availability of substrate or nutrients) after glacial retreat would have to be assessed (Filbee-Dexter et al. 2022), our results indicate that this concept also holds true for kelps. Thereby, not just summer irradiances but the cumulative annual irradiance has to be considered, when addressing the future depth distribution and biomass accumulation of photosynthetic organisms (Gattuso et al. 2006). Pedersen et al. (2020) showed that the main biomass accumulation of high-latitude *Laminaria hyperborea* is produced in spring, before the meltwater season. However, high summer irradiances are necessary to build up storage compounds for the polar night to maintain a positive annual carbon balance (Gattuso et al. 2006). Scheschonk et al. (2019) showed that

S. latissima used 96% of its storage compounds during the polar night. This implies that a reduced potential to assemble laminarin might result in a negative annual carbon balance (i.e., starvation).

Furthermore, we observed interspecific differences between the species response to high temperatures. A changed balance in competition for resources, such as light, is an important structuring factor of kelp ecosystems (Traiger and Konar 2017). This might translate into a future overlap of the realized ecological niche of *A. esculenta* with other species' habitats (e.g., *S. latissima*). The habitat model of Goldsmit et al. (2021) confirms this hypothesis, showing a higher habitat availability for *S. latissima* than *A. esculenta* in the future Canadian Arctic. As kelps are foundation species, a regime shift has cascading effects on ecosystems: important food sources, and settling- and recruitment ground for local benthic organisms might be reduced; non-indigenous and invasive species might be introduced in the ecosystem and the export production of kelp to deeper water might change. This could affect the overall productivity, light availability for the subcanopy community, biogenic habitat structure and biodiversity (Traiger and Konar 2017). Thereby, the degree of photosynthetic acclimation and thermal plasticity depends significantly on the thermal conditions during development and growth (Atkin and Tjoelker 2003; Liesner et al. 2020; Gauci et al. 2022). Hence, changes in the long-term acclimation processes will further affect kelp metabolism in future and has to be kept in mind when assessing the future kelp expansion and species composition in the Arctic.

While the loss of kelp forests as response to rising temperatures was observed at their warm-distribution edge (Krumhansl et al. 2016; Filbee-Dexter et al. 2019, 2020), major kelp forest expansions were modeled for the future Arctic (Krause-Jensen and Duarte 2014; Krause-Jensen et al. 2020; Assis et al. 2022). However, in this study, we showed that the sum of abiotic changes and their effects on kelps physiological and biochemical processes might lead to a future mismatch between resources and that local drivers can contradict kelp expansion and change the species composition in the future Arctic.

Data availability statement

Data supporting the findings of this study are openly available on the PANGAEA platform: Niedzwiedz, Sarina; Bischof, Kai (2022): Lab experiment on the effects of temperature on kelp respiration rates. PANGAEA, <https://doi.pangaea.de/10.1594/PANGAEA.951172>. Niedzwiedz, Sarina; Bischof, Kai (2022): Irradiance data at different depths and sites for field sampling in the Arctic fjord Kongsfjorden. PANGAEA, <https://doi.pangaea.de/10.1594/PANGAEA.951173>.

References

Aksnes, D. L., N. Dupont, A. Staby, Ø. Fiksen, S. Kaartvedt, and J. Aure. 2009. Coastal water darkening and

implications for mesopelagic regime shifts in Norwegian fjords. *Mar. Ecol. Prog. Ser.* **387**: 39–49. doi:10.3354/meps08120

Assis, J., E. A. Serrão, C. M. Duarte, E. Fragkopoulou, and D. Krause-Jensen. 2022. Major expansion of marine forests in a warmer Arctic. *Front. Mar. Sci.* **9**: 850368. doi:10.3389/fmars.2022.850368

Atkin, O. K., and M. G. Tjoelker. 2003. Thermal acclimation and the dynamic response of plant respiration to temperature. *Trends Plant Sci.* **8**: 343–351. doi:10.1016/S1360-1385(03)00136-5

Atkinson, M. J., and S. V. Smith. 1983. C:N:P ratios of benthic marine plants. *Limnol. Oceanogr.* **28**: 568–574. doi:10.4319/lo.1983.28.3.0568

Bartsch, I., M. Paar, S. Fredriksen, M. Schwanitz, C. Daniel, H. Hop, and C. Wiencke. 2016. Changes in kelp forest biomass and depth distribution in Kongsfjorden, Svalbard, between 1996–1998 and 2012–2014 reflect Arctic warming. *Polar Biol.* **39**: 2021–2036. doi:10.1007/s00300-015-1870-1

Bintanja, R. 2018. The impact of Arctic warming on increased rainfall. *Sci. Rep.* **8**: 16001. doi:10.1038/s41598-018-34450-3

Bintanja, R., and O. Andry. 2017. Towards a rain-dominated Arctic. *Nat. Clim. Change* **7**: 263–267. doi:10.1038/nclimate3240

Bischof, K., and others. 2019. Kongsfjorden as harbinger of the future Arctic: Knowns, unknowns and research priorities, p. 537–561. *In* H. Hop and C. Wiencke [eds.], *The ecosystem of Kongsfjorden, Svalbard. Advances of polar ecology*. Springer. doi:10.1007/978-3-319-46425-1_14

Bolton, J. J., and K. Lüning. 1982. Optimal growth and maximal survival temperatures of Atlantic *Laminaria* species (Phaeophyta) in culture. *Mar. Biol.* **66**: 89–94. doi:10.1007/BF00397259

Borum, J., M. F. Pedersen, D. Krause-Jensen, P. B. Christensen, and K. Nielsen. 2002. Biomass, photosynthesis and growth of *Laminaria saccharina* in a high-arctic fjord, NE Greenland. *Mar. Biol.* **141**: 11–19. doi:10.1007/s00227-002-0806-9

Bringloe, T. T., H. Verbruggen, and G. W. Saunders. 2020. Unique biodiversity in Arctic marine forests is shaped by diverse recolonization pathways and far northern glacial refugia. *Proc. Natl. Acad. Sci. USA* **117**: 22590–22596. doi:10.1073/pnas.2002753117

Bringloe, T. T., and others. 2022. Whole genome population structure of North Atlantic kelp confirms high-latitude glacial refugia. *Mol. Ecol.* **31**: 6473–6488. doi:10.1111/mec.16714

Constable, A. J., S. Harper, J. Dawson, K. Holsman, T. Mustonen, D. Piepenburg, and B. Rost. 2022. Cross-Chapter Paper 6: Polar regions. *In* H.-O. Pörtner and others [eds.], *Climate change 2022: Impacts, adaptation, and vulnerability. Contribution of working group II to the sixth assessment report of the intergovernmental panel on climate*. Cambridge Univ. Press.

- Laminariales) is mirrored by ecophysiological traits. *Bot. Mar.* **58**: 81–92. doi:10.1515/bot-2014-0086
- Konik, M., M. Darecki, A. K. Pavlov, S. Sagan, and P. Kowalczyk. 2021. Darkening of the Svalbard fjords waters observed with Satellite Ocean color imagery in 1997–2019. *Front. Mar. Sci.* **8**: 699318. doi:10.3389/fmars.2021.699318
- Krause-Jensen, D., and C. M. Duarte. 2014. Expansion of vegetated coastal ecosystems in the future Arctic. *Front. Mar. Sci.* **1**: 77. doi:10.3389/fmars.2014.00077
- Krause-Jensen, D., and others. 2020. Imprint of climate change on pan-Arctic marine vegetation. *Front. Mar. Sci.* **7**: 617324. doi:10.3389/fmars.2020.617324
- Krömer, S. 1995. Respiration during photosynthesis. *Annu. Rev. Plant. Physiol. Plant. Mol. Biol.* **46**: 45–70. doi:10.1146/annurev.pp.46.060195.000401
- Krumhansl, K. A., and others. 2016. Global patterns of kelp forest change over the past half-century. *Proc. Natl. Acad. Sci. USA* **113**: 13785–13790. doi:10.1073/pnas.1606102113
- Lenth, R. V. 2021. emmeans: Estimated marginal means, aka least-squares means. R package version 1.7.0. <https://CRAN.R-project.org/package=emmeans>
- Li, H., H. Xu, P. Zhang, M. Gao, D. Wang, and H. Zhao. 2017. High temperature effects on D1 protein turnover in three wheat varieties with different heat susceptibility. *Plant Growth Regul.* **81**: 1–9. doi:10.1007/s10725-016-0179-6
- Liesner, D., L. N. S. Shama, N. Diehl, K. Valentin, and I. Bartsch. 2020. Thermal plasticity of the kelp *Laminaria digitata* (Phaeophyceae) across life cycle stages reveals the importance of cold seasons for marine forests. *Front. Mar. Sci.* **7**: 456. doi:10.3389/fmars.2020.00456
- Loos, E., M. Coasta, and S. Johannessen. 2017. Underwater optical environment in the coastal waters of British Columbia, Canada. *FACETS* **2**: 872–891. doi:10.1139/facets-2017-0074
- Milner, A. M., and others. 2017. Glacier shrinkage driving global changes in downstream systems. *Proc. Natl. Acad. Sci. USA* **144**: 9770–9778. doi:10.1073/pnas.1619807114
- Munda, I. M., and K. Lüning. 1977. Growth performance of *Alaria esculenta* off Helgoland. *Helgolander Wiss. Meeresunters* **29**: 311–314. doi:10.1007/BF01614267
- Murchie, E. H., and T. Lawson. 2013. Chlorophyll fluorescence analysis: A guide to good practice and understanding some new applications. *J. Exp. Bot.* **64**: 3983–3998. doi:10.1093/jxb/ert208
- Payne, C. M., and C. S. Roesler. 2019. Characterizing the influence of Atlantic water intrusion on water mass formation and phytoplankton distribution in Kongsfjorden, Svalbard. *Cont. Shelf Res.* **191**: 104005. doi:10.1016/j.csr.2019.104005
- Pedersen, M., K. Filbee-Dexter, K. M. Norderhaug, S. Fredriksen, N. L. Frisk, C. W. Fagerli, and T. Wernberg. 2020. Detrital carbon production and export in high latitude kelp forests. *Oecologia* **192**: 227–239. doi:10.1007/s00442-019-04573-z
- Pessarrodona, A., P. J. Moore, M. D. J. Sayer, and D. A. Smale. 2018. Carbon assimilation and transfer through kelp forests on the NE Atlantic is diminished under a warmer ocean climate. *Glob. Change Biol.* **24**: 4386–4398. doi:10.1111/gcb.14303
- Pörtner, H. O., M. Lucassen, and D. Storch. 2005. Metabolic biochemistry: Its role in thermal tolerance and in the capacities of physiological and ecological function. *Fish Physiol.* **22**: 79–154. doi:10.1016/S1546-5098(04)22003-9
- Previdi, M., T. P. Janoski, G. Chiodo, K. L. Smith, and L. M. Polvani. 2020. Arctic amplification: A rapid response to radiative forcing. *Geophys. Res. Lett.* **47**: e2020GL089933. doi:10.1029/2020GL089933
- Previdi, M., K. L. Smith, and L. M. Polvani. 2021. Arctic amplification of climate change: A review of underlying mechanisms. *Environ. Res. Lett.* **16**: 093003. doi:10.1088/1748-9326/ac1c29
- R Core Team. 2021. R: A language and environment for statistical computing. R Foundation for Statistical Computing, <https://www.R-project.org/>
- Saltveit, M. E. 2019. Respiratory metabolism, p. 73–91. In E. M. Yahia [ed.], *Postharvest physiology and biochemistry of fruits and vegetables*. Elsevier.
- Scheschonk, L., S. Becker, J.-H. Hehemann, N. Diehl, U. Karsten, and K. Bischof. 2019. Arctic kelp eco-physiology during the polar night in the face of global warming: A crucial role for laminarin. *Mar. Ecol. Prog. Ser.* **611**: 59–74. doi:10.3354/meps12860
- Schild, K. M., R. L. Hawley, J. W. Chipman, and D. I. Benn. 2017. Quantifying suspended sediment concentration in subglacial sediment plumes discharging from two Svalbard tidewater glaciers using Landsat-8 and in-situ measurements. *Int. J. Remote Sens.* **38**: 6865–6881. doi:10.1080/01431161.2017.1365388
- Schlitzer, R. 2021. Ocean data view. Version 5.5.1—64 bit (Windows). <https://odv.awi.de/>
- Skogseth, R., and others. 2020. Variability and decadal trends in the Isfjorden (Svalbard) ocean climate and circulation—An indicator for climate change in the European Arctic. *Prog. Oceanogr.* **187**: 102394. doi:10.1016/j.pocan.2020.102394
- Smale, D. A. 2020. Impacts of ocean warming on kelp forest ecosystems. *New Phytol.* **225**: 1447–1454. doi:10.1111/nph.16107
- Smale, D. A., and T. Wernberg. 2013. Extreme climatic event drives range contraction of a habitat-forming species. *Proc. R. Soc. B* **280**: 20122829. doi:10.1098/rspb.2012.2829
- Stomp, M., J. Huisman, L. J. Stal, and H. C. P. Matthijs. 2007. Colorful niches of phototrophic microorganisms shaped by vibrations of the water molecule. *ISME J.* **1**: 271–282. doi:10.1038/ismej.2007.59
- Svendsen, H., and others. 2002. The physical environment of Kongsfjorden–Krossfjorden, an Arctic fjord system in Svalbard. *Polar Res.* **21**: 133–166. doi:10.3402/polar.v21i1.6479

- Teagle, H., S. J. Hawkins, P. J. Moore, and D. A. Smale. 2017. The role of kelp species as biogenic habitat formers in coastal marine ecosystems. *J. Exp. Mar. Biol. Ecol.* **492**: 81–98. doi:[10.1016/j.jembe.2017.01.017](https://doi.org/10.1016/j.jembe.2017.01.017)
- Traiger, S. B., and B. Konar. 2017. Supply and survival: Glacial melt imposes limitations at the kelp microscopic life stage. *Bot. Mar.* **60**: 603–617. doi:[10.1515/bot-2017-003](https://doi.org/10.1515/bot-2017-003)
- Verardo, D. J., P. N. Froelich, and A. McIntyre. 1990. Determination of organic carbon and nitrogen in marine sediments using the Carlo Erba NA-1500 analyzer. *Deep-Sea Res.* **37**: 157–165. doi:[10.1016/0198-0149\(90\)90034-S](https://doi.org/10.1016/0198-0149(90)90034-S)
- Vranken, S., and others. 2021. Genotype-environment mismatch of kelp forests under climate change. *Mol. Ecol.* **30**: 3730–3746. doi:[10.1111/mec.15993](https://doi.org/10.1111/mec.15993)
- Wernberg, T., K. Krumhansl, K. Filbee-Dexter, and M. F. Pedersen. 2019. Status and trends for the world's kelp forests, p. 57–78. *In* C. Sheppard [ed.], *World seas: An environmental evaluation*. Elsevier. doi:[10.1016/B978-0-12-805052-1.00003-6](https://doi.org/10.1016/B978-0-12-805052-1.00003-6)
- Wondraczek, L., M. Batentschuk, M. A. Schmidt, R. Borchardt, S. Scheiner, B. Seemann, P. Schweizer, and C. J. Brabec. 2013. Solar spectral conversion for improving the photosynthetic activity in algae reactors. *Nat. Commun.* **4**: 2047. doi:[10.1038/ncomms3047](https://doi.org/10.1038/ncomms3047)
- Wright, S. W., S. W. Jeffrey, R. F. C. Mantoura, C. A. Llewellyn, T. Bjørnland, D. Repeta, and N. Welschmeyer. 1991. Improved HPLC method for the analysis of chlorophylls and carotenoids from marine phytoplankton. *Mar. Ecol. Prog. Ser.* **77**: 183–196. doi:[10.3354/meps077183](https://doi.org/10.3354/meps077183)
- Xu, Z., F. Ji, B. Liu, T. Feng, Y. Gao, Y. He, and F. Chang. 2021. Long-term evolution of global sea surface temperature trend. *Int. J. Climatol.* **41**: 4494–4508. doi:[10.1002/joc.7082](https://doi.org/10.1002/joc.7082)

Acknowledgments

This study was conducted in the frame of the project FACE-IT (The Future of Arctic Coastal Ecosystems—Identifying Transitions in Fjord Systems and Adjacent Coastal Areas). FACE-IT has received funding from the European Union's Horizon 2020 research and innovation programme under grant agreement No. 869154. The authors thank the AWIPEV station staff and Kings Bay personnel in Ny-Ålesund 2021 and the AWI scientific diving team on Spitsbergen for the logistics and support during sampling. Furthermore, we thank Britta Iken and Andreas Suchopar (University of Bremen) for pigment and carbon to nitrogen analyses. Open Access funding enabled and organized by Projekt DEAL.

Conflict of Interest

None declared.

Submitted 22 July 2022

Revised 15 December 2022

Accepted 11 January 2023

Associate editor: David Antoine